Global Journal of Pure and Applied Mathematics.
ISSN 0973-1768 Volume 22, Number 3 (2026), pp. 517–533

https://www.ripublication.com

A higher order image denoising model using Perona–Malik diffusion term

***Abdur Rohim**[1]

[1]*Department of Mathematics, Raiganj University, West Bengal, India*

Abstract

This article proposes a PDE model of order four for image denoising. The proposed model is a combination of the Perona-Malik [12] and MMC (Marquina, Mulet, and Chan) [21] models. The proposed PDE model uses energy splitting in time and the discrete Fourier spectral method in space. At the end of our article, we provide numerical observation to test the proposed model. We conclude from the numerical results that our proposed model in this article provides better denoising performance with minimal computational time than some of the classical denoising models based on PDEs.

Keywords: Image denoising, Perona-Malik Model ; Marquina-Mulet-Chan Model, Energy Splitting, 4^{th} order PDE model.

1. INTRODUCTION

One important task in image processing is image denoising, where an image is processed to remove some unwanted data called noise. Image denoising aims is to preserve fine details like edges and framework data during removing of noise. Over the last few decades, researchers have proposed different noise-removing models that preserve the edges as well as other image information. There are several methods for handling the image denoising problems like the Stochastic technique [6] [7], Wavelet-based models [5] [8] [9], Patch-based technique [10] [11], Variations and PDE based models [12] [15] [16] [17]. The PDE-based models have gained the attention of researchers because of the rigor established theory of PDEs, in the past few decades. We can categorize the PDE-based image denoising into two classes, like non-variational type and variational type PDE models. In the variational type of models, the PDE corresponds to the Euler-Lagrange equation of a functional that has to be minimized in an admissible

Hilbert space. While the PDE, in the non-variational type of models, is proposed directly by characterization of the phenomena. Among the PDE-based models, the oldest image-denoising model is the simple heat equation. The motivation behind introducing this equation came from the classical Gaussian filtering where the noisy image convoluted with two-dimensional Gaussian kernel G_σ with

$$G_\sigma(x) = \frac{1}{2\pi\sigma^2} e^{\frac{-|x|^2}{2\sigma^2}}$$

where σ denotes the standard deviation and $x = (x_1, x_2) \in \mathbb{R}^2$. The convolution of u_0 for G_σ is same as to solve the heat equation

$$u_t = \Delta u \tag{1}$$

with $u(0, x) = u_0(x)$ up to time $t = \frac{1}{2}\sigma^2$. But the heat equation is isotropic and hence it smoothens the images in all directions equally. Thus we end up with a denoising image with blurry edges. So to overcome this shortcoming Perona and Malik(PM) [12] have come up with the anisotropic diffusion model in 1990. They modified the heat equation as:

$$u_t = div(c(|\nabla u|^2)\nabla u) \tag{2}$$

with $c(s) : [0, \infty) \to (0, \infty)$ such that $c(0) = 1$ and $c(s) \to 0$ when s goes to ∞ and $|\nabla u| = \sqrt{u_x^2 + u_y^2}$. In [12], authors have used two such functions c and they are defined as $c(s) = e^{-s^2/k^2}$ and $c(s) = \frac{1}{1+s^2/k^2}$ where k is a constant introduced for controlling the diffusion.

In the year 1992 Catte et. al. [13] identified that the Perona and Malik (PM) [12] model has two drawbacks, the first one is that it keeps noise in the edges and the second one is the non-Wellposedness of the PM Model. To overcome these two drawbacks authors have come up with a modified PDE-model in [13]. J.Wei [19] proposed another PDE model to enhance the performance of Catte et. al. [13] model.

Another problem with all the 2^{nd} order models including the PM model is the staircase effect. To get rid of the staircase effect researchers have introduced various higher-order PDE models for denoising like [16] [17] [18]. We encourage the reader for more information to [1] on higher-order models.

The minimizing functional of variational models is of the form

$$E(u) = \mathcal{R}(u) + \lambda\mathcal{F}(f - u) \tag{3}$$

where $\mathcal{R}$ is represent the regularization term, u is represent the original image, f is represent the given noisy image, Ω is represent the domain of image. We assume the

additive Gaussian noise model as $f = u + \eta$ where η represent the additive Gaussian white noise, $\mathcal{F}$ is the fidelity term and $\lambda > 0$ is a constant called fidelity parameter. The fidelity term is chosen in most models in the following form

$$\mathcal{F}(f-u) = \|f-u\|^2_{L^2(\Omega)} = \int_\Omega (f-u)^2 dx. \tag{4}$$

As per the choice, the above fidelity term is called L^2 fidelity. A successful and well-known variational type PDE model was proposed in 1992 [15]. This model is known as ROF model. In this model, the authors took the regularization function $\mathcal{R}(u)$ as follows:

$$\mathcal{R}(u) = \int_\Omega |\nabla u| dx \tag{5}$$

and L^2 the fidelity term. Applying the Euler-Lagrange equation we have:

$$div\big(\frac{\nabla u}{|\nabla u|}\big) + \lambda(f-u) = 0. \tag{6}$$

The above equation is solved as an evolution expression in the form of the following:

$$u_t = div\big(\frac{\nabla u}{\sqrt{|\nabla u|^2 + \delta^2}}\big) + \lambda(f-u) \tag{7}$$

with $u(x,0) = f(x)$ and the parameter $0 < \delta << 1$ is introduced to avoid the division by zero. For the numerical tests, we set $\delta = 0.01$.

The above model can preserve edges because near the edges $|\nabla u|$ is a little bigger than the homogeneous area and the smoothing effect will be less as $c(|\nabla u|)$ will be small and in the homogeneous region $|\nabla u|$ is small, it will act like heat equation. This denoising model is referred to as the $TV - L^2$ model. However, this model has a drawback known as the staircase effect. To overcome the staircase problem researchers have come up with various higher-order models in variational settings. In [16] Lysaker, Lundervold and Tai have proposed 4^{th} order model with taking the regularization function $\mathcal{R}(u)$ as:

$$\mathcal{R}(u) = \sqrt{u^2_{x_1x_1} + u^2_{x_1x_2} + u^2_{x_2x_1} + u^2_{x_2x_2}} \tag{8}$$

with this regularization term $\mathcal{R}(u)$, they have taken the minimization energy functional as follows:

$$E(u) = \alpha \int_\Omega \sqrt{u^2_{x_1x_1} + u^2_{x_1x_2} + u^2_{x_2x_1} + u^2_{x_2x_2}} + \frac{1}{2}\int_\Omega (f-u)^2 \tag{9}$$

The above model is known as the LLT model.
Another most important model of order four was proposed in [24] by Osher, Sole, and Vese. They have taken the minimization functional as

$$\inf_{u\in BV(\Omega)} \Big\{ \int_\Omega |\nabla u| dx + \lambda ||f-u||^2_{H^{-1}} \Big\} \tag{10}$$

Using the gradient descent equation we can find the following equation

$$u_t = -\frac{1}{\lambda}\Delta\left(\nabla.\left(\frac{\nabla u}{|\nabla u|}\right)\right) + (f-u) \tag{11}$$

The above model is referred to as $TV - H^{-1}$ denoising model. Researchers have combined the 2^{nd} and 4^{th} order models to obtain better denoising models. In [21] authors have proposed a model combining a fourth-order and a second-order model for denoising. They have chosen the regularization function $\mathcal{R}(u)$ as follows

$$\mathcal{R}(u) = \int_\Omega \left(\alpha|\nabla u| + \beta g(|\nabla u|)|\Delta u|^2\right) dx \tag{12}$$

where g is a function having constant growth at ∞. For more discussion on mathematical image processing we recommend the reader to consult with the books [1, 2] and the book [3] for digital image processing.

2. RELATED MODEL AND PROPOSED MODEL

In [12] authors have proposed an anisotropic denoising model popularly known as PM-model and it is one of the pioneering works in the field of image processing. They have proposed the following model:

$$u_t = div(c(|\nabla u|^2)\nabla u) \tag{13}$$

where the function $c(s)$ satisfies the properties (i) $c(s) \to 1$ when $s \to 0$ and $c(s) \to 0$ when s goes to ∞ which ensure to preserve edges.

A variational model for denoising is obtained by minimizing the functional of following type [21]

$$min\Big\{ \int_\Omega \Big(\alpha|\nabla u|_\delta + \mu(L(u))^2\Big)\Big\} + \frac{\lambda}{2}\|f-u\|^2_{L^2(\Omega)} \tag{14}$$

where f represents given noisy image, $|x|_\delta = \sqrt{x^2+\delta^2}$ and L is any ellipptic operators. In [21] authors have chosen $L(u) = \Delta u$. With this choice the authors [21] have modified

the minimizing functional as

$$min\Big\{ \int_{\Omega} \Big(\alpha|\nabla u|_{\delta} + \mu\Phi(|\nabla u|)(L(u))^2\Big)\Big\} + \frac{1}{2}\|f-u\|^2 \tag{15}$$

with the choice $\Phi(x) = \frac{1}{(\sqrt{x^2+\gamma})^p}, \quad p > 0$. In particular the authors have chosen $p = 3$.

Applying Euler-Lagrange equation to the equation (14) with $L(u) = \Delta u$ we get the gradient descent equation as

$$u_t = \alpha\nabla \cdot \Big(\frac{\nabla u}{|\nabla u|_{\delta}}\Big) - \mu\Delta^2 u + (f-u) \tag{16}$$

with Neumann boundary conditions.

Motivated by the work of [21, 25], we modify the fourth order term by some guiding function like it was used in the PM model. To get the benefit of PM model and higher-order model we combine the (13) and (16) as follows:

$$u_t = \nabla \cdot \Big(\frac{\nabla u}{|\nabla u|_{\delta}}\Big) - \Delta\Big(\nabla \cdot (c(|\nabla u|^2)\nabla u)\Big) + \lambda(f-u) \tag{17}$$

where c is a function, same as the PM model. Here we choose the fidelity parameter λ preceding the fidelity term instead of the regularity term. The constant δ is small and it is set as 0.01 for numerical experiment. We will solve this model using convexity splitting. The proposed model can used for restoration of images degraded by other types of noise like Poisson noise and Gamma noise, where we need to modify the fidelity term accordingly. The corresponding model can be solved using Augmented Lagrangian method or ADI method.

3. CONVEXITY SPLITTING

We will use convexity splitting to discretize the time derivative of the proposed model (17) and take the discrete Fourier transform of the time discretize scheme. To do this let us define a function $\mathcal{F}(u) = \mathcal{F}(\|\nabla u\|)$ such that $\mathcal{F}'(s) = sc(s)$ where $\mathcal{F}$ is a real-valued function. Thus we get [25]

$$\nabla_{H^{-1}}\Big(\int_{\Omega} \mathcal{F}(u)dx\Big) = \Delta(\nabla \cdot c(\|\nabla u\|)\nabla u)$$

where $\nabla_{H^{-1}}$ is represent the gradient descent w.r.t H^{-1} norm. Thus the equation (17), is obtained as the gradient flow of two energy functionals in two different norms. The first term is the gradient flow of

$$E_1(u) = \int_\Omega \mathcal{F}(u)dx$$

in H^{-1} norm and the fidelity term is the gradient descent of the functional

$$E_2(u) = \int_\Omega \{\sqrt{|\nabla u|^2 + \delta^2} + \frac{\lambda}{2}(f-u)^2\}dx$$

in L^2 norm. Now we use the convexity splitting idea to both the functional E_1, E_2. We will write E_1 and E_2 as

$$E_1(u) = E_{11}(u) - E_{12}(u)$$
$$E_2(u) = E_{21}(u) - E_{22}(u)$$

where

$$E_{11}(u) = \int_\Omega \frac{C_1}{2}\|\nabla u\|^2 dx, \quad E_{12}(u) = \int_\Omega \Big(\|\frac{C_1}{2}\|\nabla u\|^2 - \mathcal{F}(u)\Big)dx,$$

and

$$E_{21}(u) = \int_\Omega \frac{1}{2}(C_2\|\nabla u\|^2 + C_3\|u\|^2)dx,$$
$$E_{22}(u) = \int_\Omega \frac{1}{2}(C_2\|\nabla u\|^2 + C_3\|u\|^2) - \sqrt{|\nabla u|^2 + \delta^2} - \frac{\lambda}{2}(f-u)^2\Big)dx,$$

where the constants C_1, C_2, C_3 are consider in such a form that the functional $E_{ij}, i, j = 1, 2$ becomes convex. For our problem, we need to choose $C_1 > 0$, $C_2 > \frac{1}{\delta}$ and $C_3 > \lambda$. Thus the time-discretized scheme with τ as the time step size will be

$$\frac{1}{\tau}(u^{k+1} - u^k) = -\nabla_{H^{-1}}(E_{11}(u^{k+1}) - E_{12}(u^k)) - \nabla_{L^2}(E_{21}(u^{k+1}) - E_{22}(u^k))$$

which leads to

$$\frac{1}{\tau}(u^{k+1} - u^k) + C_1\Delta^2 u^{k+1} - C_2\Delta u^{k+1} + C_3 u^{k+1}$$
$$= C_1\Delta^2 u^k - C_2\Delta u^k + C_3 u^{k+1} - \Delta(\nabla \cdot c(\|\nabla u^k\|)\nabla u^k) + \nabla \cdot (\frac{\nabla u^k}{\sqrt{|\nabla u^k|^2 + \delta^2}}) + \lambda(f - u^k)$$

Multiplying both sides by τ we have

$$\begin{aligned} & u^{k+1} + C_1\tau\Delta^2 u^{k+1} - C_2\tau\Delta u^{k+1} + C_3\tau u^{k+1} \\ &= u^k + C_1\tau\Delta^2 u^k - C_2\tau\Delta u^k + C_3\tau u^k \\ &\quad - \tau\Delta\big(\nabla\cdot\big(c(\|\nabla u^k\|)\nabla u^k\big)\big) \\ &\quad + \tau\nabla\cdot\left(\frac{\nabla u^k}{\sqrt{|\nabla u^k|^2+\delta^2}}\right) + \tau\lambda(f-u^k). \end{aligned} \tag{18}$$

Taking Fourier transform on both sides and using the fact that $\widehat{\Delta u} = M\hat{u}$ we have

$$\begin{aligned} & (1 + C_1\tau M_{ij}^2 - C_2\tau M_{ij} + \tau C_3)\widehat{u_{ij}^{k+1}} \\ & = (1 + C_1\tau M_{ij}^2 - C_2\tau M_{ij} + C_3\tau)\widehat{u_{ij}^k} - \tau M_{ij}\widehat{P^k}_{ij} + \tau\widehat{\kappa^k}_{ij} + \tau\lambda(\widehat{f-u^k})_{ij} \end{aligned}$$

where $P^k = (\nabla\cdot c(\|\nabla u^k\|)\nabla u^k),\ \kappa^k = \nabla\cdot(\frac{\nabla u^k}{\sqrt{|\nabla u^k|^2+\delta^2}})$ and M_{ij} is given by,

$$M_{ij} = \frac{2}{{h_1}^2}(cos(\frac{2\pi i}{n}) - 1) + \frac{2}{{h_2}^2}(cos(\frac{2\pi j}{m}) - 1)$$

with the image size $m \times n$ and h_1, h_2 are space step size in x and y directions. For the numerical results, we have used $h_1 = h_2 = 1$. Hence

$$\widehat{u_{ij}^{k+1}} = \widehat{u_{ij}^k} + \frac{\tau\lambda(\widehat{f-u^k})_{ij} - \tau M_{ij}\widehat{P^k}_{ij} + \tau\widehat{\kappa^k}_{ij}}{1 + C_1\tau M_{ij}^2 - C_2\tau M_{ij} + C_3\tau}$$

In each iteration, we take the real part of the inverse Fourier transform of $\widehat{u_{ij}^{k+1}}$ as the solution u_{ij}^{k+1}.

4. NUMERICAL RESULTS

Here, we have reported some numerical result observed by our model based on some benchmark test images and compared the results with that of other three denoising models namely PM, $TV - L^2$, and LLT model. To compare the results, we have calculated the image quality metrics like Signal-to-noise ratio (SNR) and peak signal-to-noise ratio (PSNR). Higher the quality metric implies better the result. In PM model the parameters are set as $k = 0.1,\ \Delta t = 0.01$, ROF model as $\delta = 0.01, \Delta t = 1$, and LLT model as $\alpha = 0.1, \delta = 0.1$. For our model, we have chosen the time step size $\tau = 1$ and space step $\Delta x = \Delta y = 1$. The fidelity parameter λ is chosen as 15 for our model. We have added Gaussian noise whose SD (σ) 10 and 15 respectively.

Figure 1: Denoising results with different model respectively PM,$TV - L^2$,LLT, and Our model

In the first row of Figure 1, we have shown the Barbara image and its noisy version with noise level $\sigma = 10$ and presented the denoising results of all four models in the second row. From figure 1, it is visible that the result of the PM model is not that good. To evaluate the results, we have provided PSNR and SNR in Table 1. PSNR and SNR are higher than the other models which means the performance of our model surpasses the other three models. Also, we have noted the CPU time for all four models and observed that the PM model took less time.

Then we have considered the boat image and the denoising results of the noisy boat image with noise level $\sigma = 10$ have been presented in Figure 2. PSNR and SNR for this image are reported in Table 1 and observed that these indices are higher for our model than that of the other models. So we can conclude that the perforation of our model surpasses the remaining three models. From the data of the CPU time it can be observed that the $TV - L^2$ method takes the highest amount of time.

In Figure 3, we demonstrated the results of the Lena image obtained by the proposed model and compared them with that of PM, $TV - L^2$, and LLT model. From Table 1, it is evident that the PSNR and SNR are higher than the other models which indicates that the performance of our model surpasses other models.

Then we tested our model on the Cameraman and Peppers image. We have reported the denoising results in Figure 4 and Figure 5 respectively. From Figure 5 it is evident that our denoising result looks better. The image quality metrics are presented in Table 1. PSNR and SNR indicate that our result is better because the indicators for our model

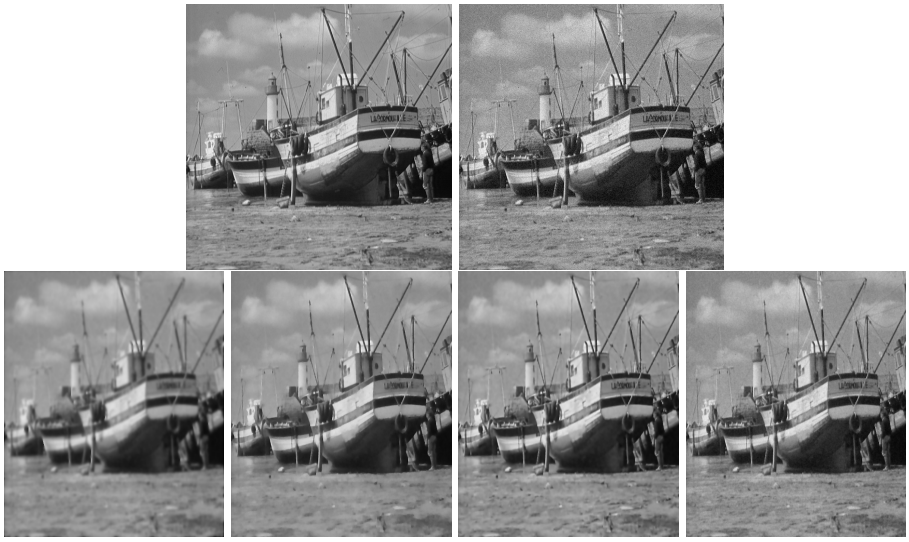

Figure 2: Denoising results with different model respectively PM,$TV-L^2$,LLT, and Our model

Figure 3: Denosing results with different model respectively PM,$TV-L^2$,LLT, and Our model

Figure 4: Denosing results with different model respectively PM,$TV-L^2$,LLT, and Our model

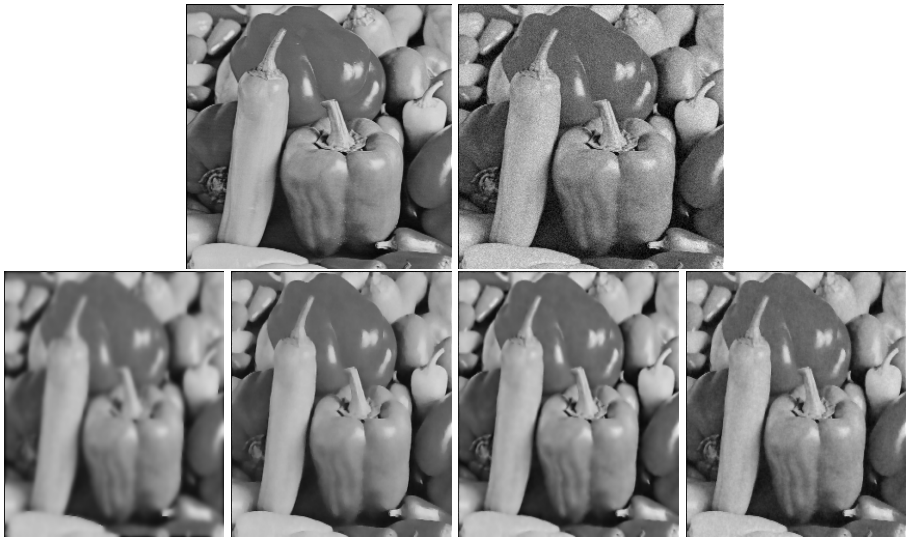

Figure 5: Denosing results with different model respectively PM,$TV-L^2$,LLT, and Our model

Image	Model	PSNR	SNR	parameters	CPU time
Barbara	PM	22.1774	16.0984	λ=10	3.30
	TV	24.8728	18.7938	λ=10	9.68
	LLT	26.4571	20.3781	α=0.1	6.46
	Our	27.2373	21.1583	λ=15	4.39
Boat	PM	24.9727	19.6301	λ=10	3.44
	TV	29.4301	24.0875	λ=10	9.80
	LLT	30.3351	24.9925	α=0.1	6.85
	Our	31.4108	26.0682	λ=15	4.47
Lena	PM	23.7771	18.1358	λ=10	0.34
	TV	28.6065	23.2783	λ=10	2.06
	LLT	28.9196	23.2783	α=0.1	0.88
	Our	30.4008	24.7595	α=15	0.41
Cameraman	PM	22.9958	17.4133	λ=10	0.27
	TV	28.4754	22.8929	λ=10	1.86
	LLT	29.0550	23.4726	α=0.1	0.86
	Our	30.1886	24.6062	λ=15	0.71
Peppers	pm	24.6794	19.0965	λ=10	0.37
	TV	30.9382	25.3553	λ=10	2.25
	LLT	30.6578	25.0749	α=0.1	0.96
	Our	32.3726	26.7897	λ=15	0.83

Table 1: Comparison of denoising results obtained using PM , $TV - L^2$ and LLT model on Real world Images with noise having standard deviation $\sigma = 10$.

are higher than those of other models. Thus the performance of our model surpasses the other three models in a reasonable time.

To check the effectiveness of our model we have added noise of higher level. We add Gaussian type of noise with SD $\sigma = 15$ repeated the experiment presented earlier. In Figure 6, we showcased the denoising outcome of the Barbara image with noise level $\sigma = 15$. PSNR and SNR for all the models have been mentioned in Table 2. From the Table, it can be observed that the performance of our model is much better than the remaining three models.

We have presented the denoised outcome of Lena image obtained by our proposed model in Figure 7 and compared them with that of PM, $TV - L^2$ and LLT Models. To check the effectiveness of various models, we have computed the image quality metric PSNR and SNR and present them in Table 2. From Table 2, it is clear that the PSNR and SNR values obtained by our model are bigger than the remaining three models which indicates that the performance of our model is much better than the remaining three. The PM model takes less time to produce the result but our model produces better results in

Figure 6: Denosing result with different model respectively PM,$TV - L^2$,LLT, and Our model

moderate CPU time.

The denoising results of the Boat and Cameraman image with noise level 15 are presented in Figure 8-Figure 9. PSNR, SNR and the CPU time taken by all the four models corresponding to Lena and Cameraman image are also tabulated in Table 2. From the Table 2, it can be observe that the performance of our model is best among all the four models. Note that the PM model is of second order and our model and LLT models are of fourth order.

The results for the Peppers image are visualized in Figure 10. The first row contains the original image and the corresponding noisy image with Gaussian noise of level $\sigma = 15$. The denoising results of PM, $TV - L^2$, LLT and our models are given in the second row. It is clear from the figure that the result of PM model is little blurry, and other results are visually better. The image quality metrics namely PSNR and SNR for all four models are presented in Table 2. From the Table, it observed that the quantity SNR and PSNR, given by our model are bigger among all the models which means that the performance of our model is better from the perspective of PSNR and SNR. The time taken by the LLT model and our model is almost the same and the $TV - L^2$ model takes the highest time among the four models to produce the result.

5. APPLICATION OF IMAGE DENOISING

There are many applications of image denoising and they are

Figure 7: Denosing result with different model respectively PM,$TV-L^2$,LLT, and Our model

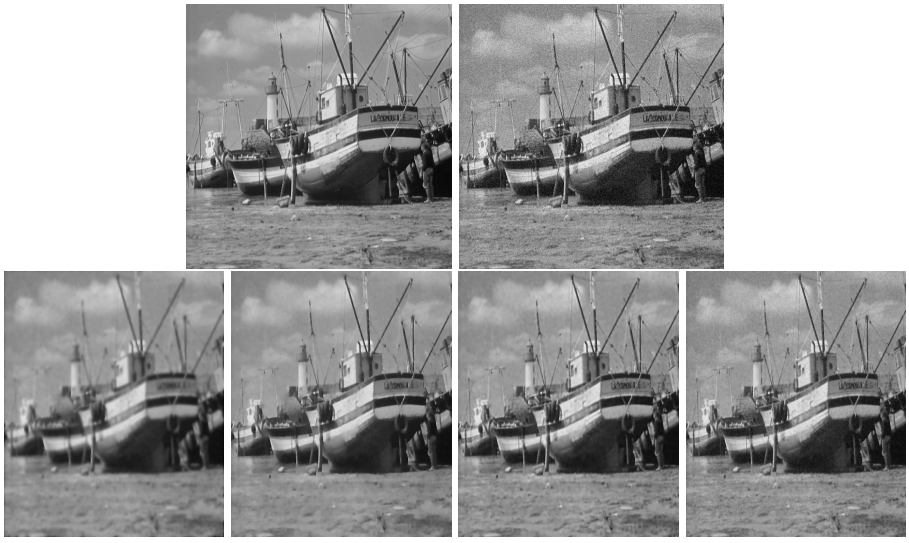

Figure 8: Denosing result with different model respectively PM,$TV-L^2$,LLT, and Our model

Figure 9: Denosing result with different model respectively PM,$TV - L^2$,LLT, and Our model

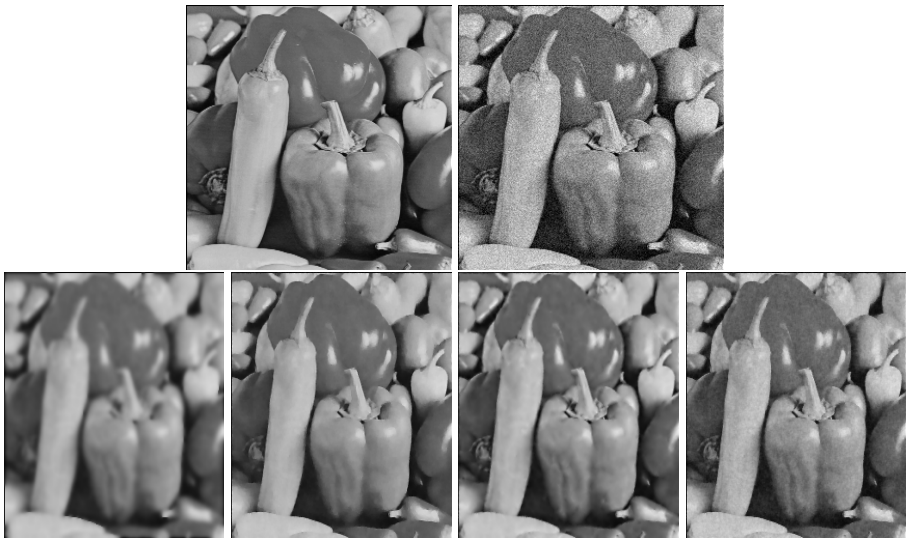

Figure 10: Denosing result with different model respectively PM,$TV - L^2$,LLT, and Our model

Image	Model	PSNR	SNR	parameters	CPU time
Barbara	PM	22.1502	16.0712	λ=10	3.36
	TV	24.8099	18.7310	λ=10	9.70
	LLT	26.3532	20.2743	α=0.1	6.46
	Our	26.6784	20.5994	λ=15	4.39
Lena	PM	23.7434	18.1021	λ=10	0.35
	TV	28.3720	22.7307	λ=10	2.05
	LLT	28.6718	23.0305	α=0.1	0.86
	Our	29.2960	23.6547	λ=15	0.84
Boat	PM	24.9134	19.5708	λ=10	3.36
	TV	29.1209	23.7783	λ=10	9.91
	LLT	29.9796	24.6370	α=0.1	7.20
	Our	30.0440	24.7014	λ=15	4.30
Cameraman	PM	22.7590	17.1766	λ=10	0.27
	TV	27.9589	22.3765	λ=10	1.84
	LLT	28.8626	22.9502	α=0.1	0.88
	Our	28.8626	23.2802	λ=15	0.69
Peppers	PM	24.5878	19.0049	λ=10	0.41
	TV	30.2641	24.6811	λ=10	2.11
	LLT	29.9986	24.4157	α=0.1	0.91
	Our	30.5211	24.9382	λ=15	0.82

Table 2: Comparison of denoising results with PM, $TV - L^2$ and LLT model on a few Real world Images with noise of level $\sigma = 15$.

1. **Medical Imaging:** Medical imaging has an important role in today's healthcare system for accurate diagnostic or better treatment purposes. Medical imaging modalities such as MRI, CT scan etc, image denoising helps to improve image quality for accurate diagnosis. It enhances the visibility of important human organ structures and reduces noise from the image.

2. **Forensics:** In the forensic investigation, images obtained from crime scenes have some defects like as noise, and image denoising helps to enhance images from crime scenes.

3. **Computer Vision:** Image denoising helps to better performance of many machine learning applications such as face recognition and image classification.

4. **Remote Sensing:** Sometimes the images obtained from the satellite contain noise due to the weather conditions. Image denoising enhances the quality of these images making it easier to analyze.

6. CONCLUSION

In our article, we have presented a PDE-based model of order four, by utilising the Perona Mallik functional for noise removal. The PDE-based model is solved using an unconditionally time stable scheme. Several numerical results on some benchmark images are presented. The numerical results indicate that the performance of our model is surprisingly better than the models like PM, LLT and $TV - L^2$ concerning PSNR, SNR. The results are obtained in moderate CPU time.

REFERENCES

[1] G. Aubert and P. Kornprobst, Mathematical problems in image processing: partial differential equations and the calculus of variations, volume 147. Springer, 2006.

[2] M. Jiang,T. F. Chan, J. Shen, Image Processing and Analysis: Variational, PDE, Wavelet, and Stochastic, in SIAM, Philadelphia, 2005.

[3] R.C. Gonzalez, and R.E. Woods, Digital Image Processing. 4th Edition, Pearson Education, New York, 2018.

[4] C.B. Schonlieb, and A. Bertozzi, Unconditionally stable schemes for higher-order inpainting, Commun. Math. Sci. vol. 9(2), pp. 413-457, 2011.

[5] D.L. Donoho, De-noising by soft-thresholding, IEEE Trans. Inf. Theory, vol. 41(3), pp. 613-627, 1995.

[6] S. Geman and D. Geman, Stochastic relaxation, Gibbs distributions, and the Bayesian restoration of images, IEEE Transactions on Pattern Analysis and Machine Intelligence, vol. 6(6), pp. 721-741, 1984.

[7] G.L. Gimel'farb, Image textures and Gibbs Random Fields, Kluwer Academic Publishers, 1999.

[8] S. Grace Chang, Bin Yu, Martin Vetterli, Adaptive wavelet thresholding for image denoising and compression, IEEE Trans. Image Processing, vol. 9(9), pp. 1532-1546, 2000.

[9] Wang XY, Yang HY, Fu ZK, A New Wavelet-based image denoising using undecimated discrete wavelet transform and least squares support vector machine, Expert System with Applications, vol. 37, pp.7040-7049, 2010.

[10] A. Buades, B. Coll, J.M. Morel, A non-local algorithm for image denoising, IEEE Computer Vision and Pattern Recognition, vol. 2, pp. 60-65, 2005.

[11] P. Chatterjee, P. Milanfar, Patch-Based Near-Optimal Image Denoising, IEEE Trans. on Image Processing, vol. 21(4), pp. 1635-1649, 2012.

[12] P. Perona, J. Malik, Scale-space and edge detection using anisotropic diffusion, IEEE Transactions on Pattern Analysis and Machine Intelligence, vol. 12(7), pp. 629-639, 1990.

[13] F. Catte and P.L. Lions and J.M. Morel and T. Coll, Image selective smoothing and edge detection by nonlinear diffusion, SIAM Journal of Numerical Analysis, vol. 29(1), pp.182-193,1992.

[14] J. Weickert, Theoretical foundations of anisotropic diffusion in image processing, Computing supplement, vol. 11, pp. 221-236, 1996.

[15] L. I. Rudin, S. Osher, and E. Fatemi, Nonlinear total variation based noise removal algorithms, Physica D, vol. 60, pp. 259-268, 1992.

[16] M. Lysaker, A. lundervold, and X.C. TAI, Noise removal using fourth-order partial differential equation with applications to medical magnetic resonance images in space and time, IEEE Trans. Image Process, vol. 12(12), pp. 1579-1590, 2003.

[17] Y. You, M. Kaveh, Fourth-order partial differential equation for noise removal, IEEE Trans. Image Processing, vol. 9(10), pp. 1723-1730, 2000.

[18] M.R. Hajiaboli, An anisotropic fourth-order diffusion filter for image noise removal, International Journal on Computer Vision, vol. 92, pp. 177-191, 2011.

[19] G. W. Wei, Generalized Perona-Malik equation for image restoration, IEEE Signal Processing Letters, vol. 6(7), pp. 165-167, 1999.

[20] Fang Li, Chaomin Shen, Jingsong Fan, Chunli Shen, Image restoration combining a total variational filter and a fourth-order filter, J. Vis. Commun. Image R., vol. 18, pp. 322-330, 2007.

[21] T. Chan, A. Marquina, P. Mulet, High-order total variation-based image restoration, SIAM J. Sci. Computing, vol. 22(2), pp. 503-516, 2000.

[22] K. Papafitsoros, C.B. Schoenlieb, B, Sengul, Combined first and second order total variation inpainting using split Bregman, Image Processing, vol. 3, pp. 112-136, 2013.

[23] Schindelin, J. Arganda-Carreras, I. and Frise, E. et al. (2012), "Fiji: an open-source platform for biological-image analysis", Nature methods 9(7): 676-682, PMID 22743772.

[24] Stanley Osher, Anders Sole, and Luminita Vese. Image decomposition and restoration using total variation minimization and the h1. Multiscale Modeling and Simulation, 1(3): 349-370, 2003. URL https://doi.org/10.1137/S1540345902416247.

[25] Q. Zou, An image inpainting model based on the mixture of Perona–Malik equation and Cahn–Hilliard equation, Journal of Applied Mathematics and Computing, vol. 66, pp. 21–38, 2021.